Journal of Electroanalytical Chemistry 694 (2013) 61–67

Contents lists available at SciVerse ScienceDirect

Journal of Electroanalytical Chemistry

journal homepage: www.elsevier.com/locate/jelechem

# Capacitive contribution to lithium storage capacity in porous $MoO_3$ films

Guangyu Zhao [b], Li Zhang [b], Kening Sun [a,b,*]

[a] State Key Laboratory of Urban Water Resource and Environment, Harbin Institute of Technology, Harbin, Heilongjiang 150090, PR China
[b] Academy of Fundamental and Interdisciplinary Sciences, Harbin Institute of Technology, Harbin, Heilongjiang 150080, PR China

ARTICLE INFO

*Article history:*
Received 11 January 2013
Received in revised form 2 February 2013
Accepted 6 February 2013
Available online 19 February 2013

*Keywords:*
Molybdenum trioxide
Porous films
Electrodeposition
Capacitive contribution
Cyclic voltammetry

ABSTRACT

Porous $MoO_3$ films are obtained by electrodepositing on Ni substrates. The galvanostatic charge/discharge tests show that, the film cathodes have a reversible capacity of 190 mA h $g^{-1}$ at a current density of 30 mA $g^{-1}$ between the voltage limits of 1.5–3.5 V vs. $Li^+$/Li, a much better performance than the pristine $MoO_3$ powder. More than 75% capacitive contribution in the capacity of porous $MoO_3$ films is responsible for the high capacity, according to the cyclic voltammetry analysis. Another improved property of the porous $MoO_3$ films is the rate performance, which still retains 70 mA h $g^{-1}$ at a current density of 1.25 A $g^{-1}$. The chronopotentiometry results reveal that, the prominent rate performances are owing to the high rate ability of the capacitive contribution.



## 1. Introduction

The possibility of applying rechargeable Li ion batteries (LIBs) in mobile and stationary power storage has generated numerous studies to improve their energy density, power density and cycling life [1–7]. It is known that the capacity of LIB is usually cathode limited, and thus, it is of great scientific and technological importance to improve the properties of cathode materials so as to enhance the performances of such batteries [7,8]. Among the numerous cathode materials, layered $MoO_3$ attracts great interest owing to the ease of the $Mo^{VI}/Mo^{V}$ couple and its layered structure. Such a layered crystal structure highly favors the reversible insertion/extraction of $Li^+$ ions into/from the host $MoO_3$ matrix [7,9]. As one of the earliest studied host materials for Li insertion, one $MoO_3$ can accommodate 1.5 Li atoms [10–12]. However, the poor kinetics of $Li^+$ diffusing in bulk layered $MoO_3$ limits its electrochemical performances [13]. Recently, $MoO_3$ nanorods [14,15], nanobelts [16] and nanofibers [17] are synthesized by various methods, and display a series of outstanding performances. The high specific surface area, good crystallinity, and possibly surface chemistry of the samples are regarded as the main reasons of their better lithium storage properties [14]. Based on these works, self-supported mesoporous $MoO_3$ film, which displays excellent performances with high energy density and high power density, is synthesized by Bruce Dunn and his coworkers [18]. The additional pseudocapacity from the ultra small grain size and the good kinetics of $Li^+$ diffusing benefited by the porous structure realize the concurrence of high energy density and high power density. Therefore, constructing self-supported porous nanocrystalline films on current collector substrates is an attractive method to improve $MoO_3$ cathode performances.

There are various strategies to construct self-supported porous nanostructures, such as hydrothermal [19], ammonia-evaporation-induced method [20], chemical vapor deposition [21], and electrodeposition [22]. Among these strategies, electrodeposition is a simple, controllable and low-cost method that can uniformly deposit thin films onto various metal substrates. In this study, electrodeposition was employed to synthesize porous $MoO_3$ films, realizing outstanding performances as LIB cathodes.

## 2. Experimental

### 2.1. Preparation of self-supported porous $MoO_3$ films

All the reagents in the experiments were analytical pure. A CHI 660D electrochemical workstation was used for electrodeposition. The electrolyte for deposition was prepared by dissolving 3.0 g Mo (2 μm, Aladdin Chemistry) powder in 100 mL $H_2O_2$ at 60 °C following the reactions:

$$2Mo + 10H_2O_2 \rightarrow Mo_2O_{11}^{2-} + 2H^+ + 9H_2O. \quad (1)$$

When the metal was completely dissolved and the exothermic reaction had ended, Pt foil was added to reduce the excess peroxide. Then the solution was adjusted to neutral with ammonia. The

* Corresponding author at: Academy of Fundamental and Interdisciplinary Sciences, Harbin Institute of Technology, Harbin, Heilongjiang 150080, PR China. Tel./fax: +86 451 86412153.
*E-mail address:* keningsun@yahoo.com.cn (K. Sun).

1572-6657/$ - see front matter © 2013 Elsevier B.V. All rights reserved.
http://dx.doi.org/10.1016/j.jelechem.2013.02.005

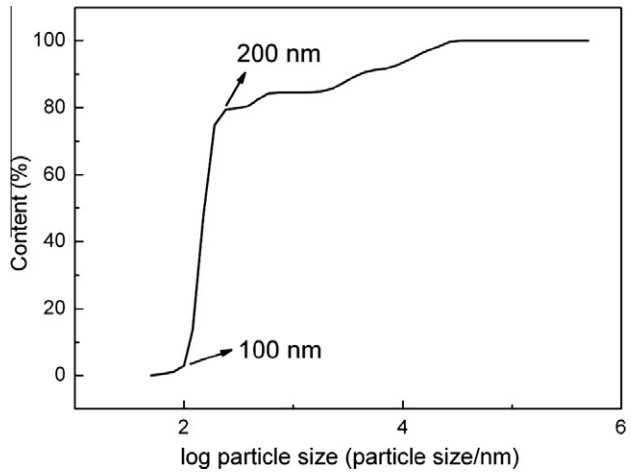


**Fig. 1.** Size distribution curve of pristine $MoO_3$ powder prepared by acid inducing deposition method.

porous $MoO_3$ films were electrodeposited at room temperature with a constant reduction current of 1 mA using 1 $cm^2$ Ni foam, a Pt foil and a saturation mercury electrode (SCE) as the working, counter and reference electrodes, respectively. The electrochemical reaction followed Eq. (2) [23]. The as-deposited films were heat-treated at 400 °C in Ar atmosphere for 3 h. The mass of the $MoO_3$ films loading on the Ni foams are near 2 mg $cm^{-2}$.

$$Mo_2O_{11}^{2-} + (2+x)H^+xe \rightarrow 2MoO_3 + \frac{8-x}{4}O_2 + \frac{2+x}{2}H_2O. \quad (2)$$

For comparison, pristine $MoO_3$ powder was prepared using precipitation method that adjusting sodium molybdate solution to acid [24]. The as-prepared $MoO_3$ powder was also heat-treated at 400 °C in Ar atmosphere for 3 h.

### 2.2. Structural and electrochemical characterization

A Hitachi SU-8100 was used to obtain scanning electron microscope (SEM) images. Transmission electron microscope (TEM) images, selected area electron diffraction (SAED) patterns and energy dispersive X-ray spectra (EDS) patterns were obtained on a FEI Tecnai $G^2$. X-ray diffraction (XRD) patterns were obtained by Rigaku D/max-2000 X-ray diffractometer with Cu Kα radiation ($\lambda$ = 1.5418 Å). Particle size analysis of the pristine $MoO_3$ powder was taken using a laser particle size analyzer (OMEC, LS 900). The mass of the electrodes were quantified by a Mettler AE240 balance.

The CHI 660D electrochemical workstation was used for the cyclic voltammetry (CV) and chronopotentiometry measurements. The battery tests were carried out in the CR2025 button testing batteries consisting of a porous $MoO_3$ film electrode, microporous membrane (Celgard 2400) and Li foil as the counter electrode. For comparison, pristine $MoO_3$ powder electrodes with area of 154 $mm^2$ coated on Cu foils were used for electrochemical measurements ($MoO_3$ powder:polyvinylidene fluoride (PVDF):carbon black = 8:1:1, weight ratio). The mass of the active material on Cu foils are about 2 mg $cm^{-2}$. The electrolyte was $LiPF_6$ (1 M) in a 50:50 (V/V) mixture of ethylene carbonate (EC) and dimethyl carbonate (DMC) provided by Tinci Company (Guangzhou China). A BTS-2000 Neware Battery Testing System was employed for charge/discharge tests.

## 3. Results and discussion

The size distribution curve of the pristine $MoO_3$ powder for comparison is shown in Fig. 1. It can be seen that most of the $MoO_3$ particles prepared by acid inducing deposition method are in the size of 100–200 nm. The surface morphology of as prepared porous $MoO_3$ films is shown in the SEM images of Fig. 2a and b. Comparing with the flat and smooth Ni substrate (the insert in Fig. 2a), the surface morphology demonstrates a continuous spread of the $MoO_3$ film with numerous nanoholes. The nanoholes may be created by the oxygen gas outflow generated in the electrochemical reaction. From the high magnification image in Fig. 2b, it is clearly seen that the nanoholes with a pore size of several decade nanometers and a hole-interval of 100–200 nm distribute in the film uniformly. The widespread nanoholes in the $MoO_3$ films can supply high speed channels for $Li^+$ ion transmission, which will play a significant role for the performances of film electrodes. Fig. 2c is the TEM images of $MoO_3$ scratched from the substrate, and the insert is a typical nanocrystal image. It can be seen that most of the nanocrystals are in the scale of several decade nanometers. This size is smaller than the $MoO_3$ particles prepared by the acid inducing deposition method, and is comparative with the diameter of nanoholes in the $MoO_3$ films. The SAED pattern in Fig. 2d can be indexed to the diffraction of orthorhombic $MoO_3$, in which the spot patterns confirm that the samples can be assigned to an orthorhombic lattice system (JCPDS: 05-0508 $a$ = 3.962 Å, $b$ = 13.858 Å, $c$ = 3.697 Å).

The XRD patterns of the films in Fig. 3a demonstrate a typical $MoO_3$ with an orthorhombic lattice, which is agreed well with the SAED results. EDS was also recorded to determine the chemical composition of $MoO_3$ nanocrystals (Fig. 3b). The results show that the nanocrystals contain only molybdenum and oxygen elements (the Cu peak is from the copper mesh).

Fig. 4a indicates the $Li^+$ insertion/extraction capacities and the coulombic efficiency of the $MoO_3$ films cycled under a current density of 30 mA $g^{-1}$ between the voltage limits of 1.5–3.5 V vs. $Li^+$/Li. From Fig. 4b, it is clearly seen that the capacity of the 1st, 2nd, 20th and 100th cycle are 376, 276, 200 and 190 mA h $g^{-1}$, respectively. Although the capacity has a sharp fading in the initial several cycles, it retains about 200 mA h $g^{-1}$ and shows a good retention in the following charge/discharge process. The coulombic efficiency increases and stabilizes at more than 98% after the initial several cycles. Another improved property of the $MoO_3$ films is the rate performances, as shown in Fig. 4c. The $MoO_3$ films realize a reversible capacity of 70 mA h $g^{-1}$, when the current density increases to 1.25 A $g^{-1}$. Furthermore, the capacity still maintains more than 170 mA h $g^{-1}$, when the current density returns to 50 mA $g^{-1}$ after cycling at the high current densities. For comparison, pristine $MoO_3$ powder was also tested in model batteries (Fig. 4d). Apparently, the $MoO_3$ films exhibits much better performances than the $MoO_3$ powder, which has a very sharp capacity fading and a bad rate performance in the subsequent high current charge/discharge. In our opinion, the major failure mechanism of the $MoO_3$ powder as anodes is the poor kinetics of $Li^+$ diffusing in bulk layered $MoO_3$ [13], which causes the $MoO_3$ powder not able to release capacity adequately at high charge/discharge currents. The reasons for the improved performances of porous $MoO_3$ film cathodes are illustrated in the following electrochemical analysis.

The CV curves of the $MoO_3$ films and $MoO_3$ powder in Fig. 5a indicate the different lithium storage mechanism and insertion/extraction properties. As to the $MoO_3$ powder electrodes, in the cathodic and anodic polarization process, two strong peaks are observed at 2.0 and 2.5 V vs. $Li^+$/Li, corresponding to the $Li^+$ intercalation processes [15,18]. According to previous reports, this charge insertion site can be described as interlayer [12]. The $MoO_3$ films exhibits a different curve shape, which has three peaks (2.7, 2.3 and 2.0 V) in the cathodic polarization process and two peaks (2.5 and 2.8 V) in the anodic polarization process. The cathodic peak at around 2.7 V vs. $Li^+$/Li can be attributed to an irreversible phase transition ($MoO_3$ into $Li_{0.25}MoO_3$), which has been shown